Development 128, 883-894 (2001)
Printed in Great Britain © The Company of Biologists Limited 2001
DEV5432

Hemicentin, a conserved extracellular member of the immunoglobulin superfamily, organizes epithelial and other cell attachments into oriented line-shaped junctions

Bruce E. Vogel* and Edward M. Hedgecock

Department of Biology, Johns Hopkins University, Baltimore, MD 21218, USA

*Author for correspondence at present address: Medical Biotechnology Center, University of Maryland Biotechnology Institute, 725 West Lombard Street, Baltimore, MD 21201, USA (e-mail: vogel@umbi.umd.edu)

Accepted 2 January; published on WWW 26 February 2001

SUMMARY

***him-4* mutations cause a novel syndrome of tissue fragility, defective cell migration and chromosome instability in *Caenorhabditis elegans*. Null mutants have abnormal escape reflex, mispositioning of the vas deferens and uterus, and mitotic chromosome loss and multinucleate cells in the germline. The *him-4* gene product, hemicentin, is a conserved extracellular matrix protein with 48 tandem immunoglobulin repeats flanked by novel terminal domains. Secreted from skeletal muscle and gonadal leader cells, hemicentin assembles into fine tracks at specific sites, where it contracts broad regions of cell contact into oriented linear junctions. Some tracks organize hemidesmosomes in the overlying epidermis. Hemicentin tracks facilitate mechanosensory neuron anchorage to the epidermis, gliding of the developing gonad along epithelial basement membranes and germline cellularization.**

Key words: Cell adhesion, Extracellular matrix, Hemidesmosome, Intermediate filaments, Nematode, *C. elegans*

INTRODUCTION

The extracellular matrix (ECM) and cytoskeleton form an integrated system controlling cell shape and movement. Cell-matrix interactions are challenging to analyze for several reasons. First, they seldom have an unambiguous polarity, i.e. cell-to-matrix versus matrix-to-cell, to simplify analysis. Second, the polymer systems that generate force and displacement are themselves responsive to mechanical stress and strain. Finally, the regulatory functions of ECM proteins are directly dependent on their structural roles. Signaling paradigms, so successful for cell growth and fate determination, provide no structural framework for understanding cell-matrix interactions. Conversely, skin fragility diseases, where tissues fracture along planes weakened by hereditary defects in ECM or cytoskeletal proteins, provide only a static structural paradigm. In fact, ECM proteins are remarkably diverse in modular composition and arrangement (Hutter et al., 2000), and likely as specialized in function. Only models that relate signaling to the unique structural properties of these proteins can explain dynamic processes of morphogenesis.

Mutations in the *him-4* locus on *Caenorhabditis elegans* chromosome X (Hodgkin et al., 1979), isolated over many years in different laboratories using a variety of mutagens and screens, cause a consistent syndrome of germline chromosome loss, defective cell migration and tissue fragility. Males and hermaphrodites in this nematode species have five autosome pairs, plus one or two X-chromosomes, respectively. Rare meiotic nondisjunction of the X-chromosome produces sporadic males, approx. 0.2%, among the self-progeny of wild-type hermaphrodites. Mutations causing more frequent loss of the X-chromosome in germline cells have a Him (for high incidence of males) phenotype. Although some mutations specifically affect X-chromosome segregation, most *him* loci affect all six chromosomes more-or-less equally. As autosomal aneuploidy is not tolerated, the latter strains produce a high fraction of inviable zygotes. We show that germline defects in *him-4* mutants include frequent mitotic chromosome loss and occasional fusion of neighboring cells.

Unique among known *him* loci, we have discovered that *him-4* has unexpected pleiotropic defects in development and behavior, characteristic of tissue fragility. As facile explanations, e.g. concerted disruption of adjacent or nested genes, had been eliminated, we cloned this locus to understand the novel association of chromosome segregation and cell adhesion phenotypes. We describe the cellular phenotypes of *him-4* and the molecular identification of hemicentin, a large extracellular member of the Ig superfamily with human orthologs, as its gene product. Secreted from skeletal muscle and gonad, hemicentin is recruited to specific extracellular sites where it forms long, fine tracks. In the gonad, a lattice of hemicentin tracks regulates cellularization of the germline syncytium. Hemicentin tracks regulate the attachment of specific mechanosensory processes on the epidermis. Other tracks regulate the attachment and movement of intestine,

uterus and vas deferens, and specific muscle cells on the epidermal basement membrane. On mechanosensory neurons and uterus, these tracks organize hemidesmosome assembly and squamification within the overlying epidermis. The cellular phenotypes of *him-4* mutants suggest hemicentin tracks are not static anchorages, but dynamic structures that facilitate directed cell movement.

MATERIALS AND METHODS

Genetics

Strains

Nematodes were routinely cultured at 20°C. Excepting *e1267*, isolated after ICR-191 treatment (Hodgkin et al., 1979), all *him-4* alleles were isolated after ethylmethanesulfonate (EMS) treatment (Sulston and Hodgkin, 1988). Alleles *n2836* and *n2837* were generous gifts from A. Chisholm. Alleles *rh166* and *rh198* were isolated in F2 colony screens for abnormal linker cell migration (Mig) phenotype. Alleles *rh303*, *rh304*, *rh305*, *rh306*, *rh307* were isolated in screens for uterine prolapse (Uta) phenotype. Alleles *rh318*, *rh319*, *rh320* and *rh321* were obtained in a non-complementation screen for Uta phenotype. Mutagenized males were mated with *dpy-6 (e14) him-4 (rh306) daf-12 (rh84)* hermaphrodites, and rare nonDpy Uta nonDaf hermaphrodite cross-progeny were cultured individually.

Aneuploidy

To relate the frequencies of males, inviable zygotes and nullo-X ova, we assume all chromosomes are equally affected, sperm and ova are equally affected, nullisomic and disomic gametes are equally frequent, and all autosomal aneuploids are inviable. Let ‘m’ denote the measured frequency of males among viable self-progeny, ‘i’ the predicted frequency of inviable zygotes, and ‘p’ the predicted frequency of nullo-X ova. Ignoring multiple events, the fraction of inviable zygotes among self-progeny caused by autosomal monosomy or trisomy (i) is 2×10p=20p and the fraction of males among viable self-progeny caused by nullo-X ova or sperm (m) is 2×p/(1-i)=2p/(1-20p). Substituting m=5-6% and solving these equations, we obtain p=1.7-1.9% and i=33-38%, respectively.

Molecular biology

Bacterial recombination

The full-length *him-4* gene was assembled from cosmids F15G9 and W07D2 using homologous recombination in *Escherichia coli* (Chartier et al., 1996). Briefly, a 4.7 kb *Sac*I-*Sma*I fragment from cosmid F15G9 and a 21.5 kb *Not*I-*Spe*I fragment from cosmid W07D2 were subcloned together into low copy number vector pWKS30 (Wang and Kushner, 1991). This construct was linearized with *Not*I and co-transformed into *E. coli* strain BJ5183 with a 20 kb *Nco*I fragment from cosmid F15G9. Recombination between the linear molecules created a circular 48 kb plasmid selected by ampicillin resistance.

Green-fluorescent protein

Using overlapping PCR primers, we inserted a unique *Sac*II restriction site into the hemicentin coding region, changing nucleotides F15G9:13,573-13,578 to ATC.TGG.CCC.GCG.GTC.TTC. The coding sequence for *Aequorea victoria* green fluorescent protein (GFP) from plasmid pPD113.54 was inserted in-frame into this restriction site (Chalfie et al., 1994).

Light and electron microscopy

DNA staining

Adult hermaphrodites were transferred to a drop of 0.5% phenoxypropanol in M9 buffer on a microscope slide and decapitated. Extruded gonads were fixed with a drop of Carnoy’s buffer (60% ethanol, 30% acetic acid, 10% chloroform), air-dried and stained for 30 minutes with 1μg/ml DAPI (Boehringer) in PBS, and washed for 5 minutes.

Membrane staining

Adult hermaphrodites were decapitated in M9 buffer and extruded gonads were placed in a suspension of DiIC18 crystals (Molecular Probes) in 3.7% formaldehyde. After 3 hours of incubation at room temperature, the tissue was stained with DAPI as described above. Stained gonads were mounted on microscope slides containing a preformed 5% agar pad.

Antibody staining

Adult worms were placed between microscope slides coated with 1% bovine serum albumin, frozen on dry ice, fractured, and fixed in methanol and acetone as described previously (Miller and Shakes, 1995).

Confocal and deconvolution microscopy

All fluorescent images were collected and processed using a Deltavision microscope system (Applied Precision) or by a Leica TCS-NT confocal microscope.

Electron microscopy

Adult hermaphrodites were fixed and embedded for serial thin-section electron microscopy according to Hall (Hall, 1995).

RESULTS

him-4 encodes a novel secreted protein

By three-factor mapping, *him-4* was localized to the *sup-28 daf-12* interval of chromosome X (see ACeDB database, http://www.sanger.ac.uk/software/Acedb/). Using restriction fragment length polymorphisms (RFLPs) between strains N2 Bristol and Rc301, we narrowed it to the 600 kb region between cosmids F58E9 and K04F12. Assaying clones from this region by germline microinjection (Mello et al., 1991), we found that overlapping cosmids F15G9 and W07D2 can rescue *him-4* mutants if introduced together, but not when injected separately. By inference, *him-4(+)* is contained entirely within these two cosmids, extending beyond the overlap region in both directions. Northern blots of total RNA using probes from this region revealed a single mRNA of about 16 kb. The *Caenorhabditis* genome consortium had previously identified potential coding sequences in this region for two large protein fragments with tandem immunoglobulin repeats. By RT-PCR, we confirmed that these fragments come from a single mRNA, comprising 62 exons, 15,811 nucleotides in length plus a 22 nucleotide trans-spliced SL1 leader and a polyA tail. As predicted, a 43 kb *Sac*I-*Spe*I fragment spanning this transcription unit, constructed by bacterial recombination, rescues *him-4* mutants.

Full-length *him-4* mRNA potentially encodes a large secreted protein (5198 residues), designated ‘hemicentin’ (Fig. 1A), mnemonic for both its approximately 50 (‘hemicentum’) structural modules and its frequent association with hemidesmosomes. Following a hydrophobic signal peptide (residues 1-24), hemicentin has a novel N-terminal domain (residues 25-433), 48 tandem Ig modules (residues 434-4837), a hydrophilic spacer (residues 4838-4947), three tandem epidermal growth factor (EGF) modules (residues 4948-5078), and a novel C-terminal domain (residues 5079-5198). The

immunoglobulin repeats resemble Ig modules of neural cell-adhesion molecule and related cell-adhesion molecules; six Ig modules (numbers 4, 24, 32, 33, 34 and 45) contain the sequence RGD, a potential binding site for integrins. In some cDNAs, exon 56 splices to an acceptor site internal to exon 57, shortening the 110 amino acid spacer between Ig and EGF domains by 23 amino acids. The first EGF motif is unusual, having only 4 cysteines; the second and third repeats resemble Ca^{2+}-binding EGF modules of Notch and related proteins. In addition to conserved cysteines within Ig and EGF repeats implicated in intramodule disulfide bonds, hemicentin has four orphan cysteines, two at either end of the molecule (Fig. 1B,C). Finally, there are no hydrophobic sequences indicative of potential transmembrane helices or GPI-anchors.

To confirm we had correctly identified the locus, we examined *him-4* alleles for possible mutations in the hemicentin coding sequence. Starting from the 5′ end, we screened successive fragments of genomic DNA (nucleotides 15,331-18662 and 19,111-21,052) using hydroxylamine cleavage of mismatched cytosines (Montandon et al., 1989). Alleles *rh319* and *rh321* contain CG-to-TA transitions at nucleotides F15G9:18,286 and F15G9:19,321, changing codons Q875 and Q1098, respectively, to UAA terminators (Fig. 1A). Presumably, most of the 13 remaining alleles contain mutations further 3′ in the hemicentin-coding sequence or, less likely, AT-to-TA transversions that are not detectable by this method.

Bodywall muscles and gonadal leader cells secrete hemicentin

To study hemicentin synthesis and assembly into extracellular matrices, we constructed transgenic strains carrying a full-length gene with GFP-coding sequence inserted in-frame between codons 34-35, immediately after the signal peptide. Because the protein is rapidly secreted from cells, tissues expressing GFP-hemicentin at low rates might escape detection. To enhance our sensitivity, we deleted codons 10-25 encoding the hydrophobic signal peptide and discarded all sequence beyond *Kpn*I:20,981. As predicted, this N-terminal protein fragment, designated ΔSP-GFP-hemicentin, is not secreted but accumulates at high levels in the cytoplasm. We examined the cellular sites of hemicentin expression at various developmental stages. Excepting bodywall muscles and gonadal leaders, described below, no other cells were observed to express ΔSP-GFP-hemicentin.

Bodywall muscles

Beginning in late embryogenesis (approx. 500 minutes), and continuing through adulthood, hemicentin is synthesized by lateral bodywall muscle cells along the entire length of the animal, excepting cells six and eight near the nerve ring (Fig. 2A). Medial bodywall muscle cells express little if any hemicentin.

Gonadal leaders (hermaphrodite)

Beginning soon after their genesis in late L1 stage, hermaphrodite distal-tip cells express hemicentin continuously throughout development (Fig. 2B). The anchor cell, or proximal leader, expresses hemicentin beginning in early L3 stage soon after cell commitment (Fig. 2C). During L4 stage, this cell fuses with other uterine cells forming the utse syncytium (Newman et al., 1996). ΔSP-GFP-hemicentin diffuses throughout the utse syncytium at this time, but it is not known whether *him-4* is transcribed in nuclei other than the anchor. In the adult, all expression within the utse syncytium ceases.

Gonadal leaders (male)

In the male, distal-tip cells never express hemicentin. The linker cell, or proximal leader, expresses hemicentin beginning at early L2 stage, soon after cell commitment (Fig. 2D). Expression continues through to late L4, when the linker cell reaches the preanal region and fuses with cloacal epidermis (Sulston et al., 1980). Downregulation of ΔSP-GFP-hemicentin expression in adult males occurs even in *him-4* backgrounds where the linker cell never reaches the cloaca (see below).

Hemicentin forms extracellular tracks connecting diverse tissues

We examined the extracellular sites of hemicentin assembly at various developmental stages using a full-length GFP-hemicentin transgene, *rhIs23*, integrated into chromosome III (Mello and Fire, 1995). This transgene complements all known

Table 1. Phenotypic comparison of *him-4* alleles

	Phenotype					
Genotype	Mna Mechanosensory neuron anchorage	Uta Uterine seam anchorage	Mig Linker migration (%±s.d.)	Him XO zygotes (%±s.d.)	Zyg Inviable zygotes (%±s.d.)	Fec Brood size (mean±s.d. (*n*))
Wild type	non-Mna	non-Uta	0±0	0.3±0.1	0.8±0.2	330±34 (8)
e1267	Mna	Uta	61±4	4.8±1.0	31±2	10±8 (21)
n2836	Mna	Uta	79±4	7.7±0.9	43±3	16±16 (33)
n2837	Mna	Uta	74±4	2.8±0.6	41±6	59±49 (15)
rh166	Mna	Uta	29±4	5.2±1.0	37±2	18±16 (30)
rh198	Mna	Uta	41±5	2.7±0.7	36±1	13±15 (42)
rh303	Mna	Uta	60±5	2.2±0.6	39±6	22±18 (29)
rh304	Mna	Uta	20±4	4.4±0.8	30±11	27±37 (24)
rh305	non-Mna	Uta	41±5	1.0±0.4	13±2	10±10 (58)
rh306	non-Mna	Uta	14±3	0±0	4±1	38±31 (21)
rh307	Mna	Uta	68±5	4.1±0.9	29±6	18±22 (28)
rh318	Mna	Uta	46±5	4.9±0.8	38±5	37±33 (20)
rh319	Mna	Uta	61±5	5.4±1.0	35±3	18±20 (29)
rh320	Mna	Uta	71±5	5.2±1.1	47±7	35±40 (11)
rh321	Mna	Uta	73±4	5.9±0.9	43±3	20±32 (35)
rh319;rhIs23	non-Mna	non-Uta	1±1	0±0	4±1	192±10 (4)

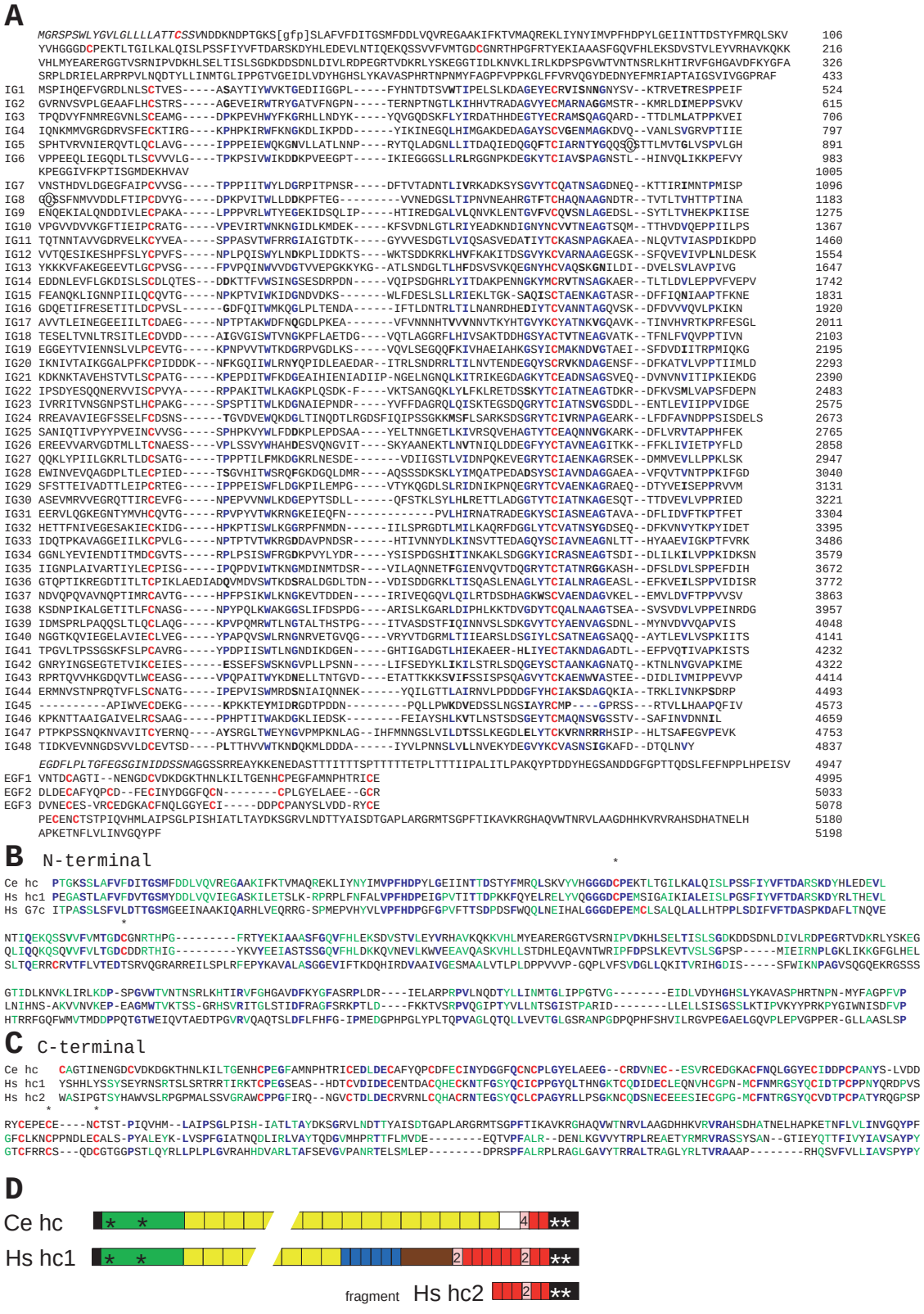

him-4 phenotypes (Table 1). Moreover, in a *him-4(+)* background, it causes no phenotypes, dominant or recessive, potentially arising from the expression of GFP-hemicentin itself or disruption of genes near the integration site. Secreted GFP-hemicentin forms fine, line-shaped extracellular tracks where specific tissues contact the basal surface of the epidermis. In addition, a lattice of hemicentin tracks forms between neighboring germline cells where they line the rachis. In general, tracks can form between cells that do not themselves express hemicentin.

Fig. 1. *C. elegans* hemicentin. (A) Predicted amino acid sequence of hemicentin (GenBank Accession Number AF074901). The predicted N-terminal signal peptide is italicized. The insertion site for green-fluorescence protein between residues 34-35 is shown [gfp]. Residues Q874 and Q1098, mutated to termination codons in *him-4* alleles *rh319* and *rh321*, respectively, are circled. Immediately after the 48 Ig repeats, an optional 23 amino acid sequence found in some RT-PCR products is italicized. (B,C) Comparison of N-terminal and C-terminal domains with human hemicentin 1 (Carpten et al., 2000; Carpten, personal communication), hemicentin 2 (B. V., unpublished observations) and G7c/NG37. (D) Proposed structural organization of *C. elegans* and human hemicentins (adapted from Carpten et al., 2000; Carpten et al., personal communication) showing the N-terminal domain (green), immunoglobulin modules (yellow), thrombospondin type 1 modules (blue), nidogen-like domain (brown), EGF modules (red) and C-terminal domain (black). For clarity, only a few of the immunoglobulin modules are shown. In the EGF repeat domain, variant or novel cysteine-rich sequences are labeled with their numbers of cysteines (pink). Conserved cysteines in the unique terminal domains are marked with asterisks.

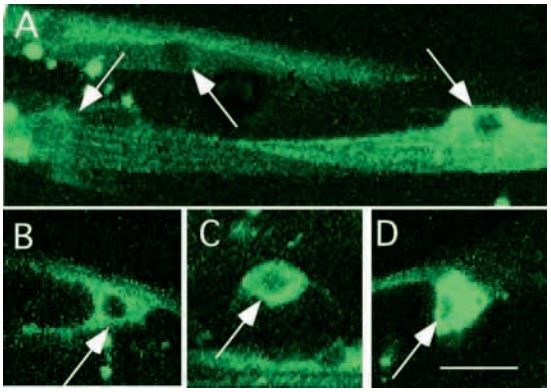

Fig. 2. Bodywall muscles and gonadal leaders secrete hemicentin. Confocal images of cells expressing ΔSP-GFP-hemicentin (arrows). (A) Dorsal aspect of adult hermaphrodite showing lateral bodywall muscle cells; no fluorescence is visible in the medial bodywall muscle cells between them. (B) Distal-tip cell in L2 stage hermaphrodite. (C) Anchor cell in L3 stage hermaphrodite. (D) Linker cell in L3 stage male. Scale bar: 10 μm.

Bodywall muscle

In all four bodywall muscles, hemicentin accumulates between the anteriormost pair of cells and the developing pharynx. By hatching, some 15-20 fine, regularly spaced, hemicentin tracks are insinuated at one end between muscle cells 1 and 2, and attached at their other end to the pharyngeal basement membrane (Fig. 3A). These tracks persist throughout postembryonic life. Spaced 2-3 μm apart, these hemicentin tracks are 7-9 μm long and 0.4-0.6 μm thick in adults. Lying within a single plane, they slope posteriorly in resting animals as they project from pharynx to muscle. During foraging and feeding, these tracks can flex as the head moves from side to side, or pivot at their ends as the pharynx moves, shifting from orthogonal, relative to pharynx and body wall, through oblique to nearly parallel.

Intestine

Hemicentin accumulates in regions immediately flanking the four bodywall muscles where the epidermis, muscle and intestine come into contact. There it forms longitudinal tracks, 1.0-1.4 μm thick, joining intestine and epidermis, and possibly intestine and bodywall muscle, across their basement membranes. Brightest along the anteriormost (int1) and posteriormost intestinal cells (int9), these eight tracks run the length of the intestine (Fig. 3B).

Neurons

Hemicentin assembles on mechanosensory neurons ALM (PLM) and AVM (PVM), ventral cord motoneurons VD1-VD13, and neurons in anterior and posterior sublateral nerves (Fig. 3C,D). Hemicentin forms continuous twin tracks, over 300 μm long and 0.2 μm thick (at most), one on either side of each axon. Center-to-center separation between these tracks increases with axon diameter, reaching about 0.4 μm in the adult for ALM (PLM) (Fig. 4A) The other axons are smaller in diameter and their hemicentin tracks are closer together and several-fold fainter. Hemicentin tracks were not observed elsewhere in the nervous systems of hermaphrodites or males. In particular, no hemicentin was associated with other classes of ventral cord motoneurons, e.g. DD, or with the nerve ring itself.

We introduced our GFP-hemicentin reporter gene into several mutants affecting determination, differentiation or function of neurons with hemicentin tracks (Chalfie and Sulston, 1981; Jin et al., 1994; Zhou and Walthall, 1998). In *mec-5 (e1340)* and *mec-9 (e1434)*, hemicentin tracks on ALM (PLM) and AVM (PVM) are normal. In *mec-1 (e1066)*, the tracks on ALM (PLM) are normal in spacing but reduced in intensity to the level of AVM (PVM) and other neurons described above (Fig. 4B). In *mec-1 mec-9* double mutants, hemicentin tracks on ALM (PLM) neurons resembled *mec-1* mutants alone. In *unc-30 (e191)*, no hemicentin accumulates on VD motoneurons, whereas in *unc-55 (e1170)*, these tracks and motor axon trajectories are normal.

Germline

By hatching, hemicentin has accumulated in the extracellular space between the germline cells. As they proliferate, hemicentin gradually disappears from lateral spaces between cells to concentrate in apical spaces that surround the central rachis. Confocal microscopy reveals a quasi-hexagonal lattice of hemicentin tracks about 3.5 μm per side and 0.3-0.5 μm thick (Fig. 3G). More proximally, after germline cells enter meiosis, the lattice of hemicentin tracks disassembles, leaving a diffuse sheet of hemicentin surrounding the rachis.

Anchor cell and uterus

In early L4 hermaphrodites, hemicentin concentrates on the utse syncytium, where it forms a broad nascent attachment with epidermal seam cells (Newman et al., 1996). During differentiation of these attachments, the zone of hemicentin narrows circumferentially until it forms a track, 65-70 μm long and 0.5-0.7 μm thick, coincident with the mature uterine-seam attachment. The hemicentin track persists at this site through to adulthood (Fig. 3E).

Linker cell and vas deferens

In late L2 males, hemicentin accumulates at the leading edge of the linker cell before it turns dorsalwards across the

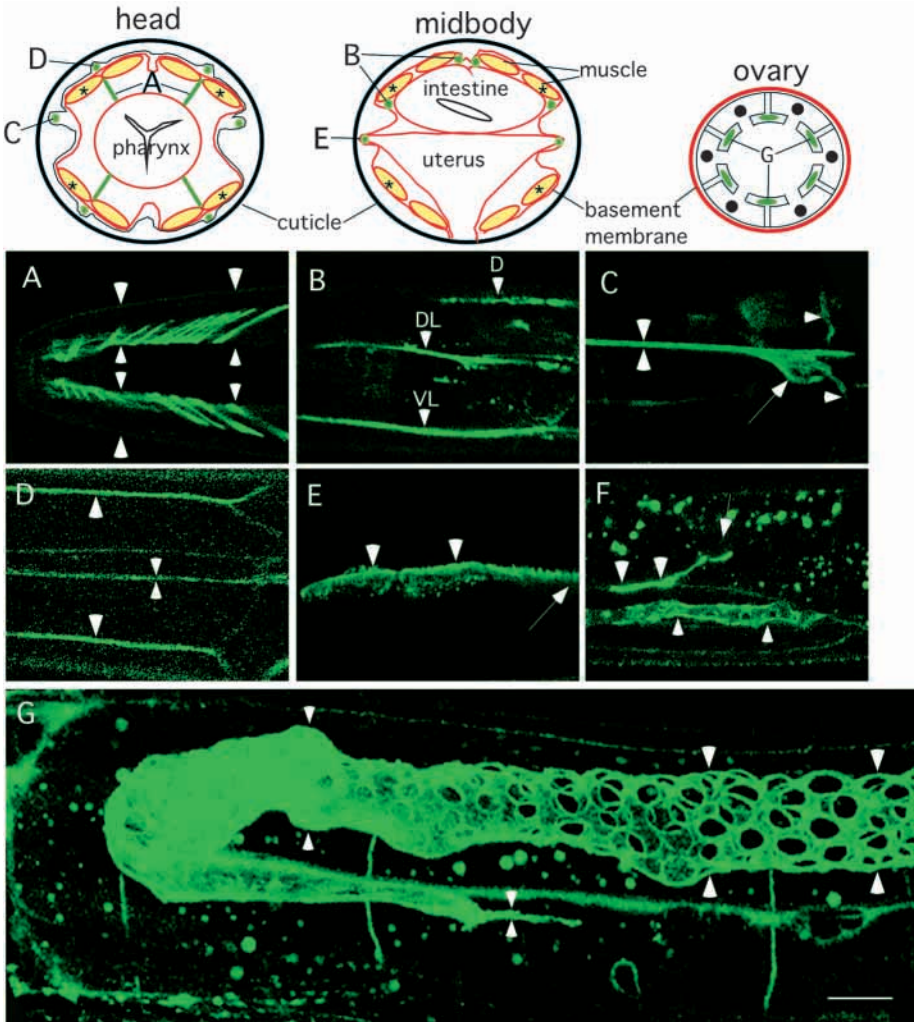

Fig. 3. Hemicentin tracks. Confocal images of GFP-hemicentin tracks. (Top) Cross-sections of bodywall and distal gonad provide the approximate positions of these tracks within the nematode. Letters refer to specific panels below. Lateral bodywall muscle cells are marked with asterisks. Except for L3 stage male in F, images are from adult hermaphrodites. (A,D) dorsal and (B,C,E-G) lateral aspects. (A) Multiple, oblique tracks joining pharyngeal basement membrane to bodywall muscle cells 1 and 2. External cuticle (large arrowheads) and pharyngeal basement membrane (small arrowheads) are marked for reference. (B) Longitudinal tracks joining intestine and epidermis (arrowheads). Flanking the bodywall muscles, these tracks run at dorsal (D), dorsolateral (DL), ventrolateral (VL) and ventral (not shown) positions. (C) Tracks on axon (large arrowheads) of ALM mechanosensory neuron (arrow). VD motoneuron commissure (small arrowheads) is also visible. (D) Tracks along SAA and SAB axons (large arrowheads) in the anterior sublateral nerves. VD motoneuron axons (small arrowheads) are also visible in dorsal nerve cord. (E) Longitudinal tracks (arrowheads) joining uterine utse cell to seam syncytium in adult hermaphrodite. Only the anterior half of the utse cell is shown; the center of the cell is marked (arrow). (F) Tracks (large arrowheads) in L3 stage male joining the basement membranes of proximal and distal arms of the reflexed gonad. The linker cell (arrow) is visible at the leading end of the proximal arm. Tracks lining the rachis (small arrowheads) are visible in the distal arm. Autofluorescent granules are visible in the intestinal cytoplasm. (G) Lattice of tracks (large arrowheads) lining the rachis of mitotic germline cells in distal ovary. More proximally, uniform sheet of hemicentin (small arrowheads) lining the rachis of maturing oocytes. Several VD motoneuron commissures (not marked) are also visible. Scale bar: 10 μm.

epidermis. As it moves dorsally, the linker cell leaves behind transient hemicentin tracks between the trailing, proximal gonad, and the epidermis and intestine (Figs 3F, 5). In L3 males, once the dorsal migration is complete, the linker cell leaves behind transient hemicentin tracks between the trailing proximal gonad, and the distal gonad, epidermis and intestine.

him-4 germline and somatic phenotypes

We examined the sites of hemicentin assembly identified above in both wild-type and *him-4* animals. In many, but not all cases, hemicentin tracks coincided with a recognized extracellular junction. All known *him-4* phenotypes correlate with specific hemicentin tracks. Conversely, most identified tracks have an associated cellular defect in *him-4* mutants.

Bodywall muscles

No defects in bodywall muscles, e.g. myofibril structure or locomotion, were observed in *him-4* mutants. Using a functional GFP-integrin βPAT-3 reporter (Gettner et al., 1995; Plenefisch et al., 2000), the integrin-based attachments of bodywall muscles to the epidermis appear normal.

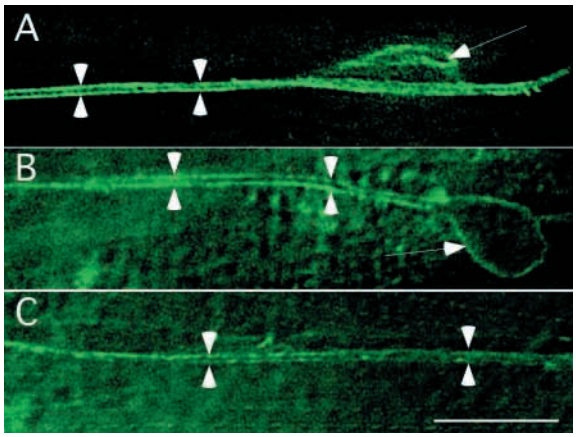

Fig. 4. Hemicentin track formation in *mec-1*. Deconvolution images of hemicentin tracks. (A,B) ALM mechanosensory neurons in wild type (A) and *mec-1 (e1066)* mutants (B). (C) VD motoraxon in dorsal nerve cord. (B,C) Pixels were re-scaled to compensate for approx. fourfold lower signal intensities. Scale bar: 10 μm.

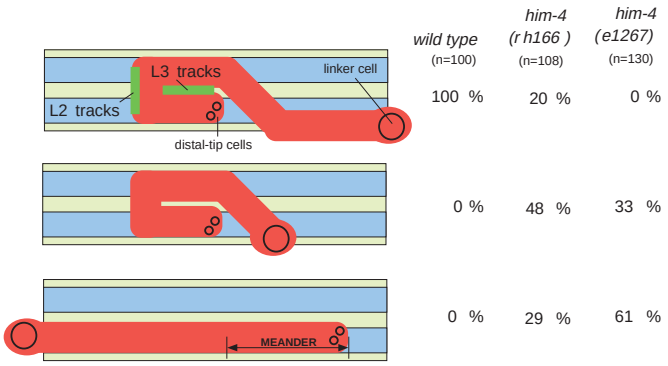

Fig. 5. Defective gonadal movements in *him-4*. Lateral aspects comparing trajectories of linker cell and trailing gonad (red) in wild-type and *him-4* males. A portion of the bodywall is shown with epidermis (yellow) and bodywall muscles (blue). Hemicentin tracks are also shown (green).

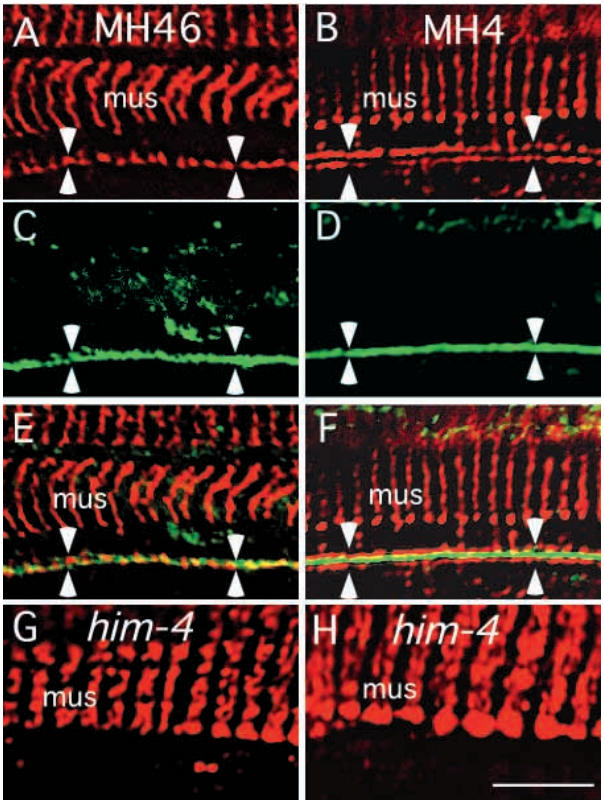

Fig. 6. Defective induction of hemidesmosomes and intermediate filaments in *him-4*. Deconvolution images comparing (A,E,G) myotactin (mAb MH46) and (B,F,H) intermediate filaments (mAb MH4) with (C-F) GFP-hemicentin (rabbit anti-GFP, Molecular Probes). Bodywall muscles (mus) and ALM neurons (arrowheads) both induce hemidesmosomes and associated intermediate filaments in the overlying epidermis, but only neurons recruit hemicentin tracks. (G,H) In *him-4 (rh319)*, bodywall muscle attachments are normal, but ALM neurons fail to induce hemidesmosomes. Scale bar: 5 μm.

Intestine

In wild-type hermaphrodites, the anterior- and posteriormost intestinal cells remain stably affixed to the bodywall during feeding and locomotion. In *him-4 (rh319)*, these cells fail to adhere or spread against the bodywall and instead slide freely within the pseudocoelom. In blind comparisons, wild-type and *him-4* hermaphrodites could be reliably sorted based on this intestinal phenotype. In rare mutant larvae (<1%), the rectum everts, arresting development.

Mechanosensory neurons

In *him-4* null mutants, ALM (PLM) processes fail to induce assembly of hemidesmosome and intermediate filament in the overlying epidermis, and squamification (Figs 6, 7D). Instead, they remain in their juvenile position adjacent the bodywall muscles, accumulating little or no extracellular mantle. These mutants respond normally to light touch with an eyebrow hair (Chalfie and Sulston, 1981). They also respond to plate tap (Chiba and Rankin, 1990), although their direction of acceleration is variable. In *him-4*, 44% (45/103) of the adults tested accelerated forwards rather than backwards, compared with only 7% (7/100) of wild type. Repeated testing of individual *him-4* hermaphrodites gave roughly equal numbers of forwards and backwards accelerations for each individual. Finally, anatomy and function of mechanosensory neurons in *mec-1 him-4* double mutants resembled *mec-1* alone.

Other neurons

Forwards and backwards locomotion appear completely normal in *him-4 (rh319)* mutants. Moreover, no defects in the axonal trajectories of VD or sublateral neurons were observed using *unc-47-gfp* and *unc-119-gfp* reporters (Maduro and Pilgrim, 1995; McIntire et al., 1997; H. Hutter and E. M. H., unpublished observations).

Germline

In ovaries of *him-4* hermaphrodites, large binucleate germline cells are frequently intermixed among mononucleate cells of normal size (Fig. 8B). Similarly, maturing oocytes occasionally have two or, rarely, more nuclei. Only 60% of hermaphrodite self-progeny are viable and 5-6% of these offspring are males (Table 1). Consistent with aneuploidy (compare with *him-6 (e1423)* arrested embryos), most of the inviable zygotes arrest postmorphogenesis. To detect autosomal aneuploid ova, we mated either wild-type or *him-6* males to *him-4 (n2836)* hermaphrodites homozygous for markers on chromosomes I (*bli-4 (e931)*), II (*rol-6 (e187)*), IV (*unc-31 (e938)*) and V (*dpy-11 (e224)*). Using *him-6* males to provide nullosomic sperm, we observed 3/781 exceptional progeny arising from disomic ova, compared with 0/1301 exceptional progeny from matings with wild-type males.

We examined DAPI-stained chromosomes in oocytes paused in diakinesis (Fig. 8C-E). In wild-type hermaphrodites, every oocyte examined had six chromosomes (n=100), presumably all bivalent. In *him-4(rh319)*, 3% had only five chromosomes (n=100), 82% had six chromosomes, 9% had seven chromosomes and 6% had eight or more chromosomes. Quantitative fluorescence measurements of cells with seven chromosomes revealed these commonly have [6:1], i.e. six bivalents plus one univalent, rather than [5:2] karyotypes. Finally, a significant fraction of the oocytes with six chromosomes have [5:1] karyotypes.

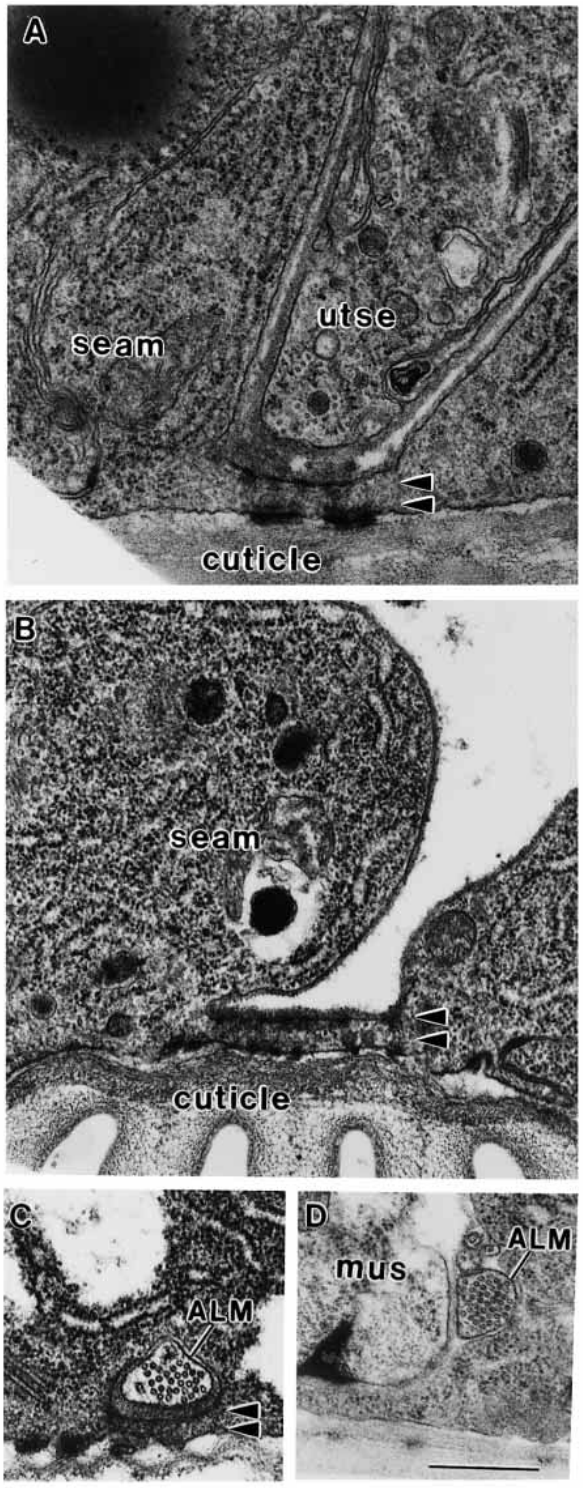

Fig. 7. Ultrastructure of hemidesmosome-based anchorages in *him-4*. Electron micrographs of uterine utse (A,B) and ALM neuron (C,D) anchorages to the epidermis in adult hermaphrodites. (A) In wild type, the utse cell forms a microtubule-filled process that runs along the basal surface of the uterus. The uterine basement membrane is thickened in this region. Squamification of the seam epidermis (arrowheads) overlying the utse cell has reduced the sheet of epidermal cytoplasm to under 200 nm in thickness. Dense material, possibly comprising hemicentin, bridges between uterine and epidermal basement in this region. Hemidesmosomes in the overlying seam cell anchor it to the epidermal basement membrane and the cuticle. (B) In *him-4 (e1267)*, the utse cell anchorage to the seam epidermis has ruptured and the uterus (not shown) has retracted. The squamified region of epidermis is broader than normal and contains many small plaques rather than a few large hemidesmosomes. (C) In wild type, the ALM process has induced hemidesmosomes formation and squamification of the overlying epidermis (arrowheads). A dense crescent of extracellular mantle lines the process channel. (D) In *him-4*, the ALM process fails to induce epidermal hemidesmosomes or accrete mantle, but instead remains at its juvenile position adjacent the bodywall muscle (mus). Scale bar: 0.5 μm.

Distal-tip cells and ovary

In *him-4* hermaphrodites, the migrations of the distal-tip cells and trailing distal gonad on the bodywall are nearly normal. Frequently, as distal-tip cells turn dorsalwards in late L3, the trailing ovary rises obliquely, rather than making an orthogonal turn. Very rarely, distal-tip cell and ovary fail to turn dorsalwards, instead continuing straight along the ventral bodywall muscles.

Anchor cell and uterus

We examined the formation of the uterine-seam attachment by DIC and fluorescence-microscopy using a functional GFP-integrin βPAT-3 reporter, and by transmission electron microscopy. In wild-type hermaphrodites, the entire attachment is visible by DIC as a continuous longitudinal line. Within this structure, regions of uterine muscle attachment are visible at either end by fluorescence of GFP-integrin on the muscle cells. In *him-4*, the initial broad interaction of uterus and epidermis fails to elongate and narrow properly so that the mature attachment is overly broad and includes only the central region. Soon after uterine muscle contractions associated with egg-laying commence, uterine-seam attachments fail and the uterus pulls away from the epidermis, splitting between their basement membranes (Fig. 7B). Resulting uterine prolapse through the vulva causes premature death of the adult hermaphrodite. The small brood sizes of these hermaphrodites, averaging only 20 viable self-progeny, reflect premature death of the gravid adult plus a smaller contribution from zygotic inviability (Table 1).

Linker cell and vas deferens

In about two-thirds of the male larvae of *him-4* null mutants, the linker cell and trailing proximal gonad fail to turn dorsalwards in late L2, and instead migrate along the ventral bodywall muscles into the head (Fig. 5; Table 1). Unexpectedly, the distal gonad meanders posteriorly along the bodywall during L4 stage in these individuals. In the remaining one-third of male larvae, the linker cell and proximal gonad complete their ventralwards movement, then halt prematurely in early L4 stage. In either case, the vas deferens fails to join the cloaca, resulting in sterility.

Allelic comparisons

All 14, recessive alleles described here are maintained as homozygous fertile strains. Zygotic *him-4(+)* expression is both necessary and sufficient for wild-type phenotype. The seven most severe alleles, which include identified nonsense mutations *rh319* and *rh321*, are indistinguishable for all traits examined and probably represent the null phenotype (Table 1).

The seven hypomorphic alleles were ranked by decreasing function for quantitative traits:

Him [wild type ≈ rh306 › rh305 › rh198, rh303, n2837 › rh319, rh321, etc.] and

Mig [wild type › rh306 › rh166, rh304 › rh198, rh305 › rh319, rh321, etc.].

Mildest for all traits examined, rh306 causes uterine prolapse (Uta phenotype) but no discernable defect in ALM (PLM) anchorage (Mna phenotype). Alleles rh166 and rh304 have severe Him (mild Mig) phenotypes, whereas rh303 and n2837 have severe Mig (moderate Him) phenotypes, reflecting some functional separation between these phenotypes. Unlike null alleles, occasional him-4 (rh166) males can mate successfully (data not shown).

DISCUSSION

Hemicentin functions at a remarkable variety of cell-cell and cell-matrix junctions. Secreted from skeletal muscle and gonad, it targets tissue attachments throughout the body, forming tracks of several shapes. Hemicentin associates with cell surfaces in the nervous system and germline, and with basement membranes elsewhere. In some places, it induces hemidesmosomes in the overlying epidermis, but in other places on this same tissue, it forms undifferentiated tracks. Finally, some hemicentin tracks are permanent, but others are strictly transient structures. Despite this variety, in all places hemicentin forms fine linear tracks with a consistent orientation relative to the tissue. Based on *him-4* phenotypes, we propose that hemicentin tracks help refine initially broad regions of cell contact into oriented, line-shaped junctions. We consider possible mechanisms of this junctional reorganization, and its mechanical advantages for specific tissues. Finally, we discuss how dynamic hemicentin tracks may support oriented tissue gliding.

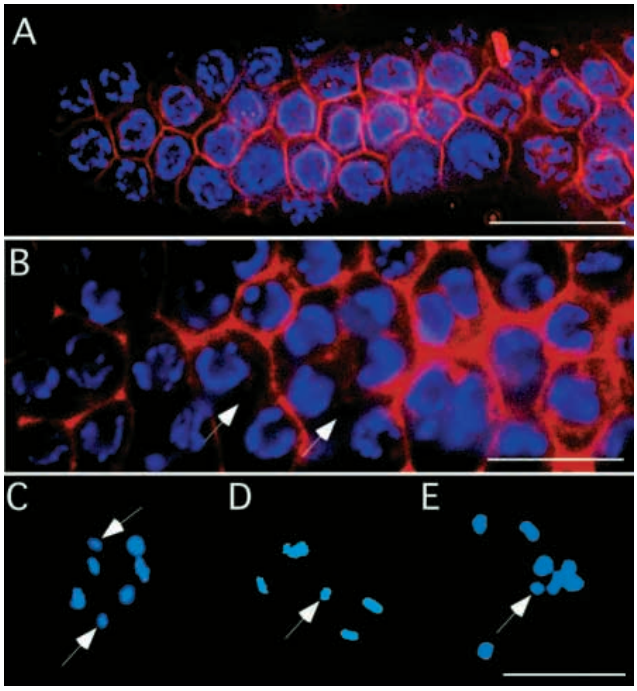

Fig. 8. Defective germline cellularization and chromosome segregation in *him-4*. (A,B) Deconvolution images of mitotic germline cells in distal ovary. Chromosomes and cell membranes are stained with DAPI (blue) and DiI (red), respectively. After prolonged staining, DiI also labels the double membranes of the nuclear envelope. (A) In wild-type hermaphrodites, mitotic germline cells are invariably mononucleate, uniform in size and regularly packed on the cortex of the ovary. (B) In *him-4 (rh319)*, mitotic germline cells often have two or more nuclei (arrows). (C-E) Chromosomes in oocytes paused at diakinesis stained with DAPI (blue). Univalent chromosomes, confirmed by signal integration (see Materials and Methods), are marked (arrows). (C) In *him-5 (e1490)*, unpaired X-chromosomes (arrows) yield a [5:2] karyotype. (D,E) In *him-4 (rh319)*, oocytes with (D) [5:1] and (E) [6:1] karyotypes are common. Scale bars: 10 μm.

Mitotic chromosome loss in *him-4* germline

The frequency of males among viable self-progeny is elevated to about 5-6% in *him-4* hermaphrodites (Table 1). Diagnostic for mitotic chromosome loss, the numbers of males produced by individual hermaphrodites shows an excess of 'jackpots' compared with independent Bernoulli trials (data not shown). The frequency of nullo-X ova, approx. 1.8%, is too low to account for so many male self-progeny, indicating hermaphrodite sperm are also affected (Hodgkin et al., 1979). The high frequency of inviable zygotes among *him-4* self-progeny, approx. 40%, plus genetic evidence for autosomal aneuploid ova, suggest all six chromosomes are similarly affected. Given 5-6% males among viable self-progeny, we predict about 1.7-1.9% nullo-X ova and 33-38% inviable zygotes, in good agreement with observation (see Materials and Methods). Frequent inviable zygotes in marked crosses of *him-4 (rh166)* males to wild-type hermaphrodites suggest male sperm are also affected (data not shown). Finally, *him-4* causes no observed chromosome loss in somatic tissues (Hedgecock and Herman, 1995), suggesting its role in chromosome segregation is limited to the germline.

Cytogenetic observations confirm that chromosome loss in *him-4* occurs during mitotic proliferation of the germline. At diakinesis, oocytes should have a [6:0] karyotype with six paired chromosomes, or bivalents, held together by one or more chiasmata, and no unpaired chromosomes, or univalents. In *him-4* hermaphrodites, occasional oocytes have only five or, rarely, four chromosomes, indicating single or double nullisomy of the primary meiocyte. By contrast, failure of pairing or crossing-over, common mechanisms of meiotic chromosome loss, give [6-n:2n] karyotypes with strictly more than six chromosomes. Finally, consistent with the male 'jackpots' described above, the karyotypes of adjacent oocytes in the ovary of a single hermaphrodite are significantly correlated.

Mitotic chromosome loss can account for all germline aneuploidy observed in *him-4* mutants. Nearly 40% of all primary meiocytes have an abnormal karyotype. From the frequency of nullisomic gametes, we estimate approximately 20-23% (1.7-1.9%×12) of all primary meiocytes have [5:1] karyotype. If mitotic nondisjuction, or 2:0 segregation, predominates over frank chromosome loss, or 1:0 segregation, we expect a similar fraction to have [6:1] karyotypes, compared with an observed 15% with seven or more chromosomes. Quantitative fluorescence measurements of DAPI-stained chromosomes to distinguish bivalents and univalents confirm the frequent occurrence of both [5:1] and [6:1] oocytes.

Hemicentin forms an extracellular scaffold for the germline syncytium

Like syncytial blastoderm of *Drosophila* embryos, cleavage furrows between proliferating germline cells in *C. elegans* are incomplete, creating a cortical layer of cells surrounding a common, cytoplasm-filled core, or rachis. In the adult hermaphrodite, mitotic germline cells act as nurses, filling the rachis with bulk cytoplasm and maternal gene products destined for extrusion into maturing oocytes. Hemicentin is not required for rachis formation per se, but helps stabilize or regulate cellularization in the germline syncytium. Incomplete isolation of neighboring spindles probably explains frequent mitotic chromosome loss found in *him-4* mutants. In particular, microtubules invading from adjacent spindles may compete for kinetochore function, occasionally capturing a chromosome. Binucleate germline cells found in these mutants indicate re-fusion of sister cells following abortive cytokinesis or sporadic fusion of neighboring cells. Multinucleate oocytes seen in the proximal ovary may reflect this mitotic error or indicate an additional role for hemicentin in oocyte maturation. Remodeling of hemicentin during meiosis suggests a role in constricting the rachis connection of immature meiocytes, ensuring bulk cytoplasm flows preferentially past them into more mature oocytes.

Mechanosensory neurons recruit hemicentin tracks

Many mechanosensory neurons have specialized endings at sheath-based sensilla beneath the cuticle (Perkins et al., 1986). By contrast, neurons that mediate escape reflexes, ALM (PLM) and AVM (PVM), are sensitive to light touch anywhere along their lengths (Chalfie and Sulston, 1981). In newly hatched larvae, ALM (PLM) processes rest on the lateral epidermis adjacent to the dorsal and ventral bodywall muscles. During larval growth, they induce the assembly of hemidesmosome and intermediate filaments in the overlying epidermis, causing local squamification (Chalfie and Sulston, 1981; Francis and Waterston, 1991). As a result, their axons are closely anchored to the cuticle along their lengths. In the adult, these hemidesmosomes form two parallel rows flanking a crescent-shaped channel between the mechanosensory processes and the epidermis. The extracellular mantle lining this channel may be related to protective mucins found in the channels of sheath-based sensilla (Perkins et al., 1986).

Wild-type adults respond consistently to light touch on anterior (posterior) body by backward (forward) acceleration, and to vibrations from plate-tapping by backward acceleration (Chalfie and Sulston, 1981; Chiba and Rankin, 1990). Mutants defective in these escape reflexes have identified 13 genes required for ALM (PLM) function (Chalfie and Sulston, 1981; Chiba and Rankin, 1990). In *mec-1*, these neurons fail to induce hemidesmosomes or squamification, remaining in their juvenile position adjacent the bodywall muscles. Two genes, *mec-5* and *mec-9*, are known to encode extracellular proteins (Du et al., 1996). In *mec-5*, the rows of hemidesmosomes overlying ALM (PLM) are occasionally interrupted (B. E. V., unpublished observations), but in *mec-9*, these epidermal anchorages appear entirely normal.

Hemicentin tracks on ALM (PLM) neurons nearly coincide with the two rows of hemidesmosomes anchoring these axons to the cuticle. In *him-4* null mutants, these neurons fail to induce hemidesmosomes or squamification, mimicking the *mec-1* anchoring phenotype. Unexpectedly, *him-4* has nearly normal touch response, indicating mechanosensation is largely separable from anchorage to the cuticle. Conversely, hemicentin still assembles on these neurons in *mec-1*, but its tracks are significantly reduced in intensity. In summary, hemicentin has no direct role in mechanotransduction, but MEC-1 has an essential, anchorage-independent role. Moreover, hemicentin can target to neurons and form tracks independently of MEC-1, but induction of hemidesmosomes in the overlying epidermis requires a functional interaction between these proteins. A model incorporating these observations is shown in Fig. 9.

The advantage of anchoring mechanosensory processes to the cuticle for improved sensitivity or directional selectivity may increase with body size. The robust anchorages of ALM (PLM) neurons to the cuticle in *C. elegans* adults have only a modest impact on behavior. Whereas wild-type juveniles accelerate in either direction to escape plate-tap, adults consistently accelerate backwards (Chiba and Rankin, 1990). This behavioral change may reflect the maturation of the ALM (PLM) anchorages, i.e., *him-4* adults retain both the juvenile anatomy and the juvenile behavior pattern. We speculate other neuronal hemicentin tracks in this small nematode species are vestiges of anchorages important in their larger ancestors. AVM (PVM) may induce a few, small hemidesmosomes, but VD motoneurons and sublateral nerves have no epidermal specializations (White et al., 1986). Relaxation and contraction of the bodywall during locomotion may modulate some ventral cord or sublateral motoneurons in nematodes (compare with

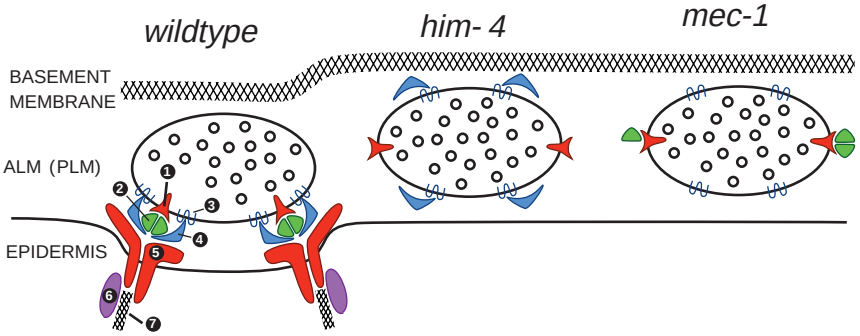

Fig. 9. Model of hemicentin function in ALM (PLM) neurons. Integrin or other (1) receptors on the ALM (PLM) neurons bind (2) hemicentin secreted from nearby skeletal muscles and nucleate track formation. A complex of (3) membrane and (4) extracellular proteins required for mechanotransduction assembles on the neurons; this complex is MEC-1 dependent and hemicentin independent. Concentrated on the epidermal surface through interaction with the hemicentin tracks, this complex recruits (5) membrane proteins myotactin and myonectin and possibly (6) cytoplasmic adaptors. In association with (7) keratin-like intermediate filaments, these hemidesmosomes anchor the neuronal processes to the cuticle and cause local squamification of the epidermis. In *him-4*, the mechanotransduction complex is normal but mislocalized, and no hemidesmosomes are induced. In *mec-1*, the mechanotransduction complex is defective, hemicentin tracks are fainter and no hemidesmosomes are induced.

Chalfie et al., 1985). Possibly, hemicentin-associated neurons are generally mechanosensitive, but we have found no behavioral or cytological defects in *him-4* that are attributable to neurons other than ALM (PLM).

Hemicentin functions across basement membranes

Hemicentin functions in basement membrane-independent attachments between germline cells and their common rachis, and between neurons and epidermis. Everywhere else, it functions across basement membranes separating two tissues. In most such places, the separation between basement membranes is small, as little as 100 nm, and the relation of hemicentin to the cell surfaces and basement membranes is uncertain. However, where hemicentin tracks couple pharynx and skeletal muscles in the head, the separation between tissues is several μm. Most or all hemicentin molecules in these tracks lie strictly between the basement membranes. By inference, hemicentin is polymerized with some matrix component, possibly itself, not directly bound to cell surfaces or even basement membrane. Interestingly, the nascent basement membranes of pharynx and bodywall muscles are directly apposed when these tracks are formed during embryogenesis (C. Norris, personal communication). We speculate that the multiple oblique tracks arise through fragmentation of a single, continuous track as these tissues separate.

Hemicentin organizes some hemidesmosomes

The nematode integument, a continuous epithelium-forming cuticle on its apical face and supporting nervous system, musculature and other tissues on its basal face, comprises the epidermis, pharynx and several interfacial epithelia. For mechanical integrity, keratin-like intermediate filaments span the integument from apical to basal faces, anchored to cuticle and basement membrane at hemidesmosomes based on non-integrin receptors (Hresko et al., 1999; M. Bercher, J. Wahl, B. E. Vogel, C. Lu, E. M. Hedgecock and J. D. Plenefisch, unpublished observations; L. Hong, T. Elbl, C. Franzini-Armstrong, J. Ward, K. K. Rybicka, B. K. Gatewood and E. Bucher, unpublished observations). In the pharynx, cytoplasmic intermediate filaments form thick, irregular tonofilaments (Albertson and Thomson, 1976), but they adopt a more regular arrangement in squamified epidermis (Francis and Waterston, 1991). Reminiscent of keratinocyte maturation in vertebrates, the distance between basal and apical cell surfaces collapses to only 150 nm in squamified regions. The mechanism of squamification is unknown. However, the distance between apposing hemidesmosome plaques is close to the fundamental repeat of intermediate filaments, suggesting filaments alternating between apical and basal hemidesmosomes pull the two faces together much like boot laces.

Several tissues induce the formation of hemidesmosomes and intermediate filaments, causing local squamification of the epidermis where they contact its basal surface or basement membrane. As a result, these cells are closely anchored to the cuticle. On ALM (PLM) neurons and utse syncytium, hemicentin tracks are required to induce epidermal hemidesmosomes or organize their pattern. In *him-4*, these anchorages are reduced or absent, causing minor defects in mechanosensation and catastrophic prolapse of the uterus during egg-laying. Hemicentin is not an obligate structural component of other epidermal anchorages. Bodywall muscles induce identical changes in the overlying epidermis without recruiting hemicentin tracks, and, as predicted, these anchorages are normal in *him-4* mutants.

Vertebrate homologs of hemicentin

Recently, a human ortholog of hemicentin has been identified in chromosome 1q24-25 by genomic sequencing (Carpten et al., 2000; Carpten et al., personal communication); several human hereditary diseases have been linked to this chromosome region (Carpten et al., 2000; Tsukaguchi et al., 2000). The N-terminal domain, which is most highly conserved, is 43% (165/388) identical in amino acid sequence to nematode hemicentin, including both cysteines (Fig. 1B). The central region contains 44 tandem Ig modules, six thrombospondin-type 1 modules and eight EGF modules. Examination of the expressed sequence tag database, reveals a second potential human ortholog in chromosome 9q34, designated hemicentin-2 (Fig. 1C). Finally, a human paralog, sharing only the N-terminal domain of hemicentin, has been identified within the major histocompatibility complex class region in chromosome 6p21.3. Designated G7c/NG37, this locus encodes a presumptive secreted protein (852 residues) of unknown function. Curiously, the two cysteines within the region of similarity occur at nonconserved positions (Fig. 1B).

Like other basement membrane genes (Hutter et al., 2000), the basic function of hemicentin in tissue morphogenesis has probably been conserved from nematodes to humans. Hemicentin has undergone at least two rearrangements since the phyletic separation some 600 million years ago (Fig. 1D). In the nematode lineage, a deletion near the 3′ end of the gene removed all of the thrombospondin modules and many of the EGF modules. A separate duplication in the nematode lineage, or deletion in the chordate lineage, accounts for the greater number of Ig modules in *C. elegans* hemicentin. Finally, the separation of hemicentin 1 and hemicentin 2 may reflect a subsequent gene duplication within the chordate lineage.

Models of hemicentin function

Hemicentin could form a rod-like protein about 200 nm in length with conserved cysteines at either end forming intramolecular disulfide bonds, or perhaps intermolecular bonds with other hemicentin chains or yet unidentified partners (Fig. 1D). Like other ECM proteins, hemicentin diffuses freely when first secreted. For example, well before any expression from gonadal cells, germline cells can recruit hemicentin from nearby skeletal muscles. Identified transcription factors, e.g., UNC-30, control hemicentin recruitment to specific classes of cells. Hemicentin receptors on these cells are yet unknown but might include RGD-binding integrins. Hemicentin forms long linear tracks, no more than 200 nm wide (the resolution limit of light microscopy) on neurons. Track formation probably entails interactions of hemicentin with itself, and possibly other matrix components. A preliminary experiment indicates different hemicentin domains are probably responsible for tissue targeting and track formation (B. E. V., unpublished observations). Hemicentin tracks on mechanosensory neurons can induce hemidesmosomes in the overlying epidermis (Fig. 9). MEC-1 and perhaps MEC-5 are likely effectors on these neurons, whereas myotactin and myonectins are possible receptors on epidermal cells (Du et al., 1996; Hresko et al., 1999; Hutter et al., 2000; M. Bercher, J. Wahl, B. E. Vogel, C.

Lu, E. M. Hedgecock and J. D. Plenefisch, unpublished observations; L. Hong, T. Elbl, C. Franzini-Armstrong, J. Ward, K. K. Rybicka, B. K. Gatewood and E. Bucher, unpublished observations). Finally, hemicentin tracks can be dispersed or disassembled during movement and remodeling.

Nascent cell attachments can mature and strengthen in various ways. In some cases, the region of contact broadens isotropically, producing a uniform surface of attachment or a field of punctate or focal attachments. In polarizing epithelia, the region of attachment narrows anisotropically, producing a belt-shaped adherens junction separating basolateral and apical faces. We have described a new geometry of junctional maturation into oriented line-shaped junctions, based on the track forming protein hemicentin. This organization has clear mechanical advantages for some tissues over isotropic attachments. Coupling of internal epithelia, e.g., intestine and uterus, to the bodywall by discrete, longitudinal tracks, rather than uniformly, provides mechanical purchase while allowing free filling and emptying of their lumens. Unexpectedly, hemicentin tracks deposited by gonadal leader cells are found at the regions of greatest, rather than least, relative tissue movement. In males, for example, the proximal gonad elongates and reflexes within the body cavity, pulled by its linker cell and simultaneously pushed by the proliferating germline (see Antebi et al., 1997). Without hemicentin tracks, the linker cell is unable to reorient the trailing gonad, or later pull it to the cloaca. We speculate that hemicentin tracks are not generally static anchorages, but facilitate passive movement, or gliding, of tissues along their axes.

We thank Andrew Fire, David Hall, Jonathan Hodgkin, Harald Hutter, Stephanie Leavitt, Carolyn Norris and Mark Van Doren for helpful discussions throughout this work; Andrew Chisholm for donating *him-4* alleles; Andrew Fire and Sidney Kushner for providing plasmid vectors; and Michael Sepanski for EM sectioning. This work was funded by grants from the Muscular Dystrophy Association and the National Institutes of Health. Some nematode strains used in this work were provided by the *Caenorhabditis* Genetics Center, which is funded by the NIH National Center for Research Resources.

REFERENCES

Albertson, D. G. and Thomson, J. N. (1976). The pharynx of *Caenorhabditis elegans*. *Phil. Trans. R. Soc. Lond.* **275**, 299-325.

Antebi, A., Norris, C. R., Hedgecock, E. M. and Garriga G. (1997). Cell and growth cone migrations. In *The Nematode Caenorhabditis elegans II*, (e.d. D.L. Riddle, T. Blumenthal, B. J. Meyer and J. R. Priess), pp. 583-609. New York: Cold Spring Harbor Press.

Carpten, J. D., Makalowska, I., Robbins, C. M., Scott, N., Sood, R., Connors, T. D., Bonner, T. I., Smith, J. R., Faruque, M. U., Stephan, D. A., Pinkett, H. et al. (2000). A 6-Mb high-resolution physical and transcription map encompassing the hereditary prostate cancer 1 (HPC1) region. *Genomics* **64**, 1-14.

Chalfie, M. and Sulston, J. (1981). Developmental genetics of the mechanosensory neurons of *Caenorhabditis elegans*. *Dev. Biol.* **82**, 358-370.

Chalfie, M., Sulston, J. E., White, J. G., Southgate, E., Thomson, J. N. and Brenner, S. (1985). The neural circuit for touch sensitivity in *Caenorhabditis elegans. J. Neurosci*. **5**, 956-964.

Chalfie, M. Tu, Y., Euskirchen, G., Ward, W. W. and Prasher, D. C. (1994). Green fluorescent protein as a marker for gene expression. *Science* **263**, 802-805.

Chartier, C., Degryse, E., Gantzer, M., Dieterle, A., Pavirani, A. and Mehtali, M. (1996). Efficient generation of recombinant adenovirus vectors by homologous recombination in *Escherichia coli. J. Virol.* **70,** 4805-4810.

Chiba, C. M. and Rankin, C. H. (1990). A developmental analysis of spontaneous and reflexive reversals in the nematode *Caenorhabditis elegans. J. Neurobiol.* **21**, 543-554.

Du, H., Gu, G., William, C. M. and Chalfie, M. (1996). Extracellular proteins needed for *C. elegans* mechanosensation. *Neuron* **16**, 183-194.

Francis, R. and Waterston, R. H. (1991). Muscle attachment in *Caenorhabditis elegans. J. Cell Biol.* **114**, 465-479.

Gettner, S., Kenyon, C. and Reichardt, L. F. (1995). Characterization of β*pat-3* heterodimers, a family of essential integrin receptors in *C.elegans. J. Cell Biol.* **129**, 1127-1141.

Hall, D. H. (1995). Electron microscopy and three-dimensional image reconstruction. *Methods Cell Biol*. **48**, 396-436.

Hedgecock, E. M. and Herman, R. K. (1995). The *ncl-1* gene and genetic mosaics of *Caenorhabditis elegans*. *Genetics* **141**, 989-1006.

Hodgkin, J., Horvitz, H. R. and Brenner, S. (1979). Nondisjunction mutants of the nematode *Caenorhabditis elegans*. *Genetics* **91**, 67-94.

Hresko, M. C., Schriefer, L. A., Shrimankar, P. and Waterston, R. H. (1999). Myotactin, a novel hypodermal protein involved in muscle-cell adhesion in *Caenorhabditis elegans*. *J Cell Biol.* **146**, 659-672.

Hutter, H., Vogel, B. E., Plenefisch, J. D., Norris, C. R., Proenca, R. B., Spieth, J., Guo, C., Mastwal, S., Zhu, X., Scheel, J. and Hedgecock, E. M. (2000). Conservation and novelty in the evolution of cell adhesion and extracellular matrix genes. *Science* **287**, 989-994.

Jin, Y., Hoskins, R. and Horvitz, H. R. (1994). Control of type-D GABAergic neuron differentiation by *C. elegans* UNC-30 homeodomain protein. *Nature* **372**, 780-783.

Maduro, M. and Pilgrim, D. (1995). Identification and cloning of *unc-119*, a gene expressed in the *Caenorhabditis elegans* nervous system. *Genetics* **141**, 977-988.

McIntire, S. L., Reimer, R. J., Schuske, K., Edwards, R. H. and Jorgensen, E. M. (1997). Identification and characterization of the vesicular GABA transporter. *Nature* **389**, 870-876.

Mello, C. C., Kramer, J. M., Stinchcomb, D. and Ambros, V. (1991) Efficient gene transfer in *Caenorhabditis elegans. EMBO J.* **10**, 3939-3970.

Mello, C. and Fire, A. (1995). DNA transformation. *Methods Cell Biol.* **48**, 451-482.

Miller, D. M. and Shakes, D. C. (1995) Immunofluorescence Microscopy. *Methods Cell Biol*. **48**, 365-394.

Montandon, A. J., Green, P. M., Gianelli, F. and Bentley, D. R. (1989). Direct detection of point mutations by mismatch analysis: application to hemophilia B. *Nucleic Acids Res*. **17,** 3347-3358.

Newman, A. P., White, J. G. and Sternberg, P. W. (1996). Morphogenesis of the *C. elegans* hermaphrodite uterus. *Development* **122,** 3617-3626.

Perkins, L. A., Hedgecock, E. M., Thomson, J. N. and Culotti, J. G. (1986). Mutant sensory cilia in the nematode *Caenorhabditis elegans*. *Dev. Biol.* **117**, 456-487.

Plenefisch, J. D., Zhu, X. and Hedgecock, E. M. (2000). Fragile skeletal muscle attachments in dystrophic mutants of *Caenorhabditis elegans*. *Development* **127**, 1197-1207.

Sulston, J. E., Albertson, D. G. and Thomson, J. N. (1980). The *Caenorhabditis elegans* male: postembryonic development of nongonadal structures. *Dev. Biol.* **78**, 542-576.

Sulston, J. and Hodgkin, J. (1988). In *The Nematode Caenorhabditis elegans* (ed. W.B. Wood), pp. 587-606. Cold Spring Harbor, NY: Cold Spring Harbor Laboratory Press.

Tsukaguchi H., Yager H., Dawborn, J., Jost, L., Cohlma, J., Abreu, P. F., Pereira, A. B. and Pollak, M. R. (2000). A locus for adolescent and adult onset familial focal segmental glomerulosclerosis on chromosome 1q25-31. *J. Am. Soc. Nephrol*. **11**, 1674-1680.

Wang, R. F. and Kushner, S. R. (1991). Construction of versatile low-copy-number vectors for cloning, sequencing and gene expression in *Escherichia coli. Gene* **100,** 195-199.

White, J. G., Southgate, E., Thomson, J. N. and Brenner, S. (1986). The structure of the nervous system of the nematode *Caenorhabditis elegans*. *Phil. Trans. R. Soc. Lond.* **314**, 1-340.

Zhou, H. M. and Walthall, W. W. (1998). UNC-55, an orphan nuclear hormone receptor, orchestrates synaptic specificity among two classes of motor neurons in *Caenorhabditis elegans*. *J. Neurosci.* **18**, 10438-10444.